

Impact of Time-Resolved Entropy Measurement on a One-and-One-Half-Stage Axial Turbine Performance

M. Mansour

N. Chokani

A. I. Kalfas¹

R. S. Abhari

Department of Mechanical and Process Engineering,
LSM, Laboratory for Energy Conversion,
ETH Zürich,
Zurich 8092, Switzerland

An accurate assessment of unsteady interactions in turbines is required, so that this may be taken into account in the design of the turbine. This assessment is required since the efficiency of the turbine is directly related to the contribution of unsteady loss mechanisms. This paper presents unsteady entropy measurements in an axial turbine. The measurements are conducted at the rotor exit of a one-and-one-half-stage unshrouded turbine that is representative of a highly loaded, high-pressure stage of an aero-engine. The unsteady entropy measurements are obtained using a novel miniature fast-response probe, which has been developed at ETH Zurich. The entropy probe has two components: a one-sensor fast-response aerodynamic probe and a pair of thin-film gauges. The probe allows the simultaneous measurement of the total temperature and the total pressure from which the time-resolved entropy field can be derived. The measurements of the time-resolved entropy provide a new insight into the unsteady loss mechanisms that are associated with the unsteady interaction between rotor and stator blade rows. A particular attention is paid to the interaction effects of the stator wake interaction, the secondary flow interaction, and the potential field interaction on the unsteady loss generation at the rotor exit. Furthermore, the impact on the turbine design of quantifying the loss in terms of the entropy loss coefficient, rather than the more familiar pressure loss coefficient, is discussed in detail. [DOI: 10.1115/1.4003247]

1 Introduction

Considerable resources are invested in improving the efficiency of turbomachines. Wisler [1] noted that in order to justify the return on investment, technology programs must focus on issues that most impact the costs such as hardware costs, product redesign costs, and repair cycle time. In order to reduce the overall engine length, one approach for a new turbine design is to increase the blade loading while keeping the efficiency and lifetime at their high levels. It is well known that the unsteady interaction of the rotor and stator blade rows affects the performance of axial-flow turbomachines [2–6]. For turbines with low aspect ratio and high blade loading, it has been shown (Sharma et al. [2]) that the flow is dominated by secondary flow interactions. The periodic unsteadiness is prevalent and can cause a decrease in efficiency and high-cycle fatigue of engine components. In that context, it is crucial to be able to accurately predict the losses attributed to unsteady blade row interactions.

The blade losses are quantified in terms of a loss coefficient; the stagnation pressure loss coefficient

$$\gamma = \frac{\bar{p}_{o,w1} - p_{o,w2}}{0.5 \cdot \rho \cdot w_{2,max}^2} \quad (1)$$

is commonly used. This ratio of the loss of stagnation pressure to a reference dynamic pressure can be related to the loss generation within the blade row (Greitzer et al. [7]). For steady flows, the losses can be related to changes in the stagnation pressure. However, in turbomachines, the flow is inherently unsteady, and both the relative stagnation pressure and the relative stagnation tem-

perature can change (Denton [8]). It follows that the loss coefficient should be expressed in terms of entropy (Eq. (2)), which accounts for both temperature and pressure changes,

$$\Delta s = c_p \ln \frac{T_o}{T_{o,ref}} - R \ln \frac{p_o}{p_{o,ref}} \quad (2)$$

In that regard, the correct measure of the loss is then the entropy loss coefficient (Eq. (3)),

$$\zeta = \frac{T_2 \cdot \Delta s}{0.5 \cdot w_{2,max}^2} \quad (3)$$

which appropriately accounts for the unsteady losses that arise from temporal and spatial variations in the stagnation pressure and stagnation temperature.

Only a few attempts of measuring entropy in turbomachines are reported in the literature. Ng and Epstein [9] were the first to use an aspirating probe to measure entropy in a transonic compressor. Payne et al. [10] subsequently used an aspirating probe in a high-pressure turbine stage. Brouckart [11] also used an aspirating probe but did not attempt to derive entropy measurements. In spite of these attempts, the fragility of hot wires is well known, and there are concerns about routinely using an aspirating probe in the harsh environment of a turbomachine. Buttsworth et al. [12] used thin-film heat transfer gauges in conjunction with a fast-response aerodynamic probe to measure both the unsteady total pressure and the unsteady total temperature in a turbomachine but did not attempt to derive entropy measurements as the two probes were not integrated. The use of a pair of thin-film gauges in a transient mode to derive total temperature measurements has been demonstrated by Buttsworth and Jones [13], Passaro et al. [14], and Chana [15]. An alternate approach is used in the novel miniature fast-response entropy (FENT) developed at ETH Zurich (Mansour et al. [16]). The probe integrates two components: a fast-response aerodynamic probe and a pair of thin-film gauges. This paper presents detailed unsteady entropy measurements that were made

¹Present address: Aristotle University of Thessaloniki, Greece.

Contributed by the International Gas Turbine Institute (IGTI) of ASME for publication in the JOURNAL OF TURBOMACHINERY. Manuscript received April 21, 2009; final manuscript received November 6, 2010; published online June 23, 2011. Editor: David Wisler.

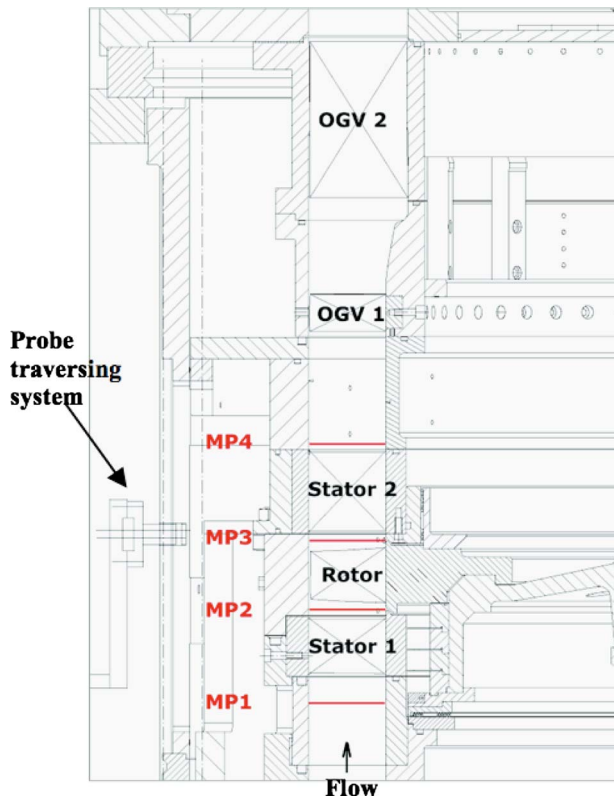


Fig. 1 Cross-section view of 1.5-stage turbine section. The probe measurement planes and tandem exit guide vane sections are also shown.

at the rotor exit of a one-and-one-half-stage unshrouded turbine that is representative of a highly loaded, high-pressure stage of an aero-engine. These measurements thus provide a unique set of experimental data.

The two objectives of the present work are as follows. The first is to quantify the losses in terms of stagnation pressure loss and entropy loss coefficients and to demonstrate that the entropy loss coefficient provides a correct measure of the turbine performance. It is also shown that the magnitude and distribution of losses can be different between the two loss coefficients. The second objective is to use the novel miniature fast-response entropy probe to quantify the impact of the inter-blade-row interaction on the modulation of the unsteady loss at the rotor exit flow field. The role of the stator wake interaction, the secondary flow interaction, and the potential field interaction on this modulation is detailed.

2 Test Rig and Measurement Setup

The experiments were performed in an axial one-and-one-half-stage turbine facility, which allows probe measurements, as shown schematically in Fig. 1. The air loop of the facility is of a quasi-closed type and includes a radial compressor, a two-stage water-to-air heat exchanger, and a calibrated Venturi nozzle for mass flow measurements. Before the flow enters the turbine section, it passes through a 3 m long straight duct, which contains flow straighteners to ensure an evenly distributed inlet flow field. Downstream of the turbine, the air loop is open to atmosphere. The turbine entry temperature is controlled to an accuracy of 0.3%, and the rotor speed is kept constant within $\pm 0.5 \text{ min}^{-1}$ by the dc generator. The pressure drop across the turbine is stable within 0.3% for a typical measurement. The main parameters of the facility are summarized in Table 1, and more information on the test rig can be found in Behr et al. [17].

For the present investigation, the turbine test case models a low aspect ratio, highly loaded, high-pressure subsonic aero-engine

Table 1 Main parameters of “LISA” 1.5-stage axial turbine research facility at design operating point

Rotor speed (rpm)	2700
Pressure ratio (1.5-stage, total-to-static)	1.60
Turbine entry temperature ($^{\circ}\text{C}$)	55
Total inlet pressure (bar)	1.4
Mass flow (kg/s)	12.13
Shaft power (kW)	292
Hub/tip diameter (mm)	660/800
First stage	
Pressure ratio (first stage, total-to-total)	1.35
Degree of reaction	0.39
Loading coefficient $\psi = \Delta h / u^2$	2.36
Flow coefficient $\phi = c_x / u$	0.65
Reynolds number at rotor exit based on true chord and blade row relative exit velocity	3.8×10^5

turbine stage. The geometry of blade row is in the public domain and available from Behr et al. [17]. Bypass air from the compressor is injected through the hub rim seal at the rotor inlet to simulate coolant air that prevents the ingestion of hot flow into the cavity between the stator and rotor disks.

A four-axis numerically controlled automatic traversing system with high precision is used to automatically position the fast-response entropy probe. The probe is inserted radially from the casing, and for circumferential positioning, the casing ring is traversed together with the probe.

The measurements were made with a recently developed FENT probe (Mansour et al. [16]). The data included in the present paper focus on the rotor exit plane (shown as measurement plane MP3 in Fig. 1). A close-up view of the tip of the FENT probe is shown in Fig. 2. The probe has a diameter of 1.8 mm and is comprised of two parts: first, a miniature silicon piezoresistive chip that is glued beneath a pressure tap to measure the unsteady static and total pressures; second, a pair of thin-film gauges, which are operated as resistance thermometers at two different film temperatures and used to measure the unsteady total temperature.

Each measurement plane is resolved by a grid of 43 measurement points in the radial direction, which are clustered close to the end wall, and 41 equally spaced points in the circumferential direction, covering one stator pitch. The serpentine shaped thin films cover a rectangular area of $1.77 \times 0.85 \text{ mm}^2$. The radial distance covered by the serpentine shaped thin films, which is 2.52% of the passage height in the measurement plane, is the minimum spatial resolution on the measurement grid. The measurements have a radial spacing of 1.125 mm in the regions of clustering and of 2.25 mm elsewhere. In the data processing, coincident phase-locked measurements of p_0 and T_0 are used to determine the unsteady relative entropy. The measurement bandwidth is 40 kHz, and data are acquired at a sampling frequency of 200 kHz over a period of 2 s. The uncertainties in the measurements and derived quantities are summarized in Table 2.



Fig. 2 Photograph of the tip of the unsteady entropy probe

Table 2 Summary of measurement uncertainties

Parameter	Relative uncertainty (%)
P_{ref}	0.016
T_{ref}	0.12
P_0	0.1
T_0	2.5
Δs	2.51

3 Measurement of Loss Generation Through the Rotor

The spanwise distribution of the pitchwise-averaged relative stagnation pressure and entropy loss coefficients are shown in Fig. 3. The respective overall losses are 11.2% in terms of the entropy loss coefficient and 19% in terms of the stagnation pressure loss coefficient. It is evident that overall losses are overestimated by more than 69% using the stagnation pressure loss coefficient.

As the blades have a low aspect ratio, the secondary flow extends over in a wide range between the casing and the hub. The rotor hub and tip passage vortices are located in the ranges of 4.2–31.5% and 57–81% blade spans, respectively. The hub passage vortex is less marked but extends over a larger spanwise extent than the tip passage vortex because of the use of the injection at the hub rim seal between the first stator and rotor rows. This injection is described by Schuepbach et al. [18]. In Fig. 3, the presence of the tip leakage vortex (TLV) can also be clearly identified between the 81% span and the casing and is the region of highest losses.

Figure 4 shows a loss audit based on the entropy and stagnation pressure loss coefficient distribution. Following the approach of Chaluvadi et al. [19], the span was divided into four regions, as summarized in Table 3. The spanwise extents of these regions are inferred from the loss coefficient distributions shown in Fig. 3 and are detailed as follows. The TLV region extends from 81% to 100% span. The upper passage vortex (UPV) region covers 57–81% span, and the wake region lies between 31.5% and 57% spans. The remainder span comprises the lower passage vortex region, LPV, and extends from 4.2% to 31.5% span. The region does not extend from the hub wall as the first measurement point of the coincident pressure and temperature is 2.94 mm away from the hub wall.

The loss generation audit shows the relative losses in each region as a percent fraction of the total loss across the span. It is

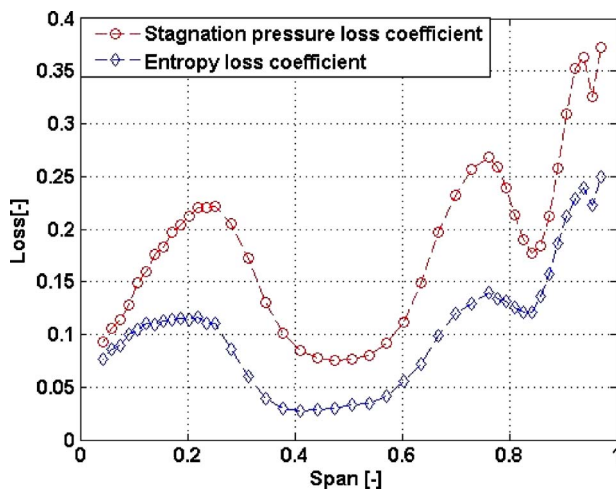


Fig. 3 Pitchwise-averaged spanwise distribution of entropy and relative stagnation pressure coefficient at rotor exit

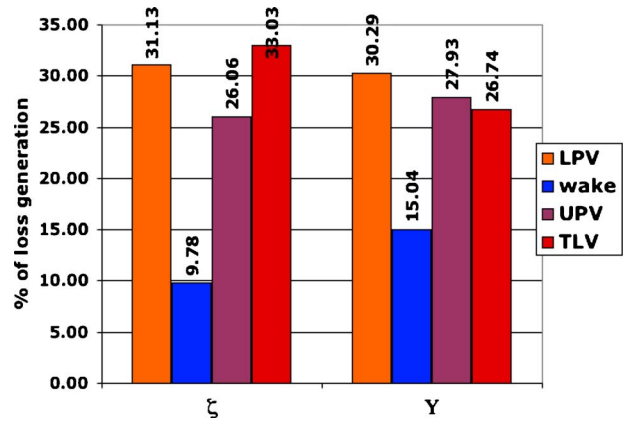


Fig. 4 Entropy loss coefficient, ζ , stagnation pressure loss coefficient, Y , and loss audits based on pitchwise-averaged measurements

evident that the entropy and stagnation pressure loss coefficients show different relative distributions of loss generation. The entropy loss coefficient identifies the tip leakage vortex as the most lossy region (33.03%) followed by the lower passage vortex (31.13%) and the upper passage vortex (26.06%). On the other hand, in terms of the stagnation pressure loss coefficient, the regions of decreasing loss generation are the lower passage vortex (30.29%), the upper passage vortex (27.93%), and the tip leakage vortex (26.74%). The significance of these differences is that from the perspective of a designer, the tip leakage, which is the most lossy region, would not be identified as such if the pressure loss coefficient is used to evaluate the loss generation. Although both coefficients identify the wake region as that with the lowest loss generation, 9.78% and 15.04% in terms of the entropy and stagnation pressure, respectively, we note that the impact of the higher blade loading is more significant when evaluated using the former coefficient compared with the latter. In the subsequent section of the paper, the unsteady interactions at the rotor exit are detailed. These unsteady interactions have received much attention in the past. However, clearer insight is now provided through the use of the FENT probe that has been developed in the context of the present work.

4 Time-Resolved Flow Field

The unsteady rotor-stator interactions result in variations in the total pressure and total temperature. Time snapshots, at $t/T = 0.86$, of the total pressure and total temperature flow fields at the rotor exit are shown in Fig. 5. The measurements cover one stator pitch, with the leading edge of the second row stator located at the midpitch (pitch=0). The flow fields are dominated by the secondary flows. As the blade surfaces are adiabatic, it can be seen that the work done on the rotor by the rotor secondary flows is less than that done by the freestream since the rotor secondary flows have a total temperature that is about 4% above that of the freestream. In a later section, time-space diagrams are used to

Table 3 Spanwise extents of regions at rotor exit used in the loss generation audit analysis

Region	Range (% of blade span)
TLV	81–100
UPV	57–81
Wake	31.5–57
LPV	4.2–31.5

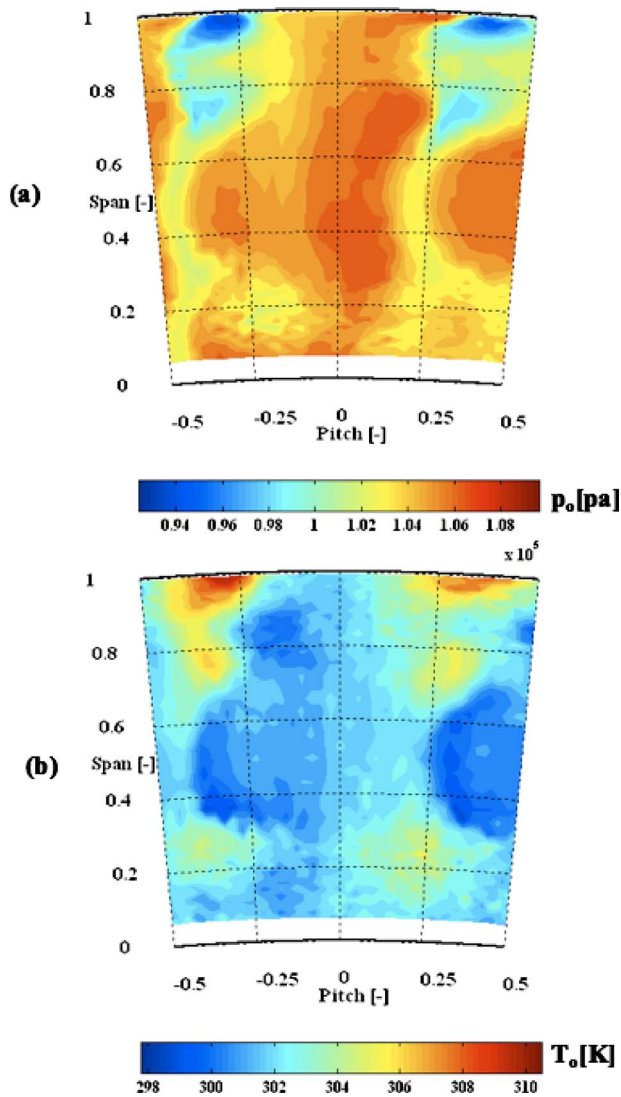


Fig. 5 Time-resolved (a) total pressure and (b) total temperature distribution at rotor exit

describe the time-varying behavior of the stator 1 wake. The first law of thermodynamics can be written in the form

$$\frac{Dh_o}{Dt} = \frac{1}{\rho} \frac{\partial p}{\partial t} = C_p \frac{DT_o}{Dt} \quad (4)$$

This form illustrates that as the total enthalpy decreases, a stationary observer sees a pressure and a total temperature that decrease with time. The ratios of the total pressure and total temperature deficits between the stator 1 wake and the surrounding freestream as they flow through the rotor stage are $\Delta p_{ow}/\Delta p_{of}=0.71$ and $\Delta T_{ow}/\Delta T_{of}=0.76$. The former ratio is in good agreement with the measurement of Schuepbach et al. [20], who used a fast-response aerodynamic probe in the same configuration. Moreover, the stator wake has a total temperature excess compared with the surrounding freestream at the rotor inlet, creating a total temperature excess at the rotor exit. Overall, these measurements suggest that the work done on the rotor by the stator 1 wake is less than that done by the freestream.

The corresponding time snapshots of the pressure loss coefficient and entropy loss coefficient are shown in Fig. 6. It is seen that, in general, the stagnation pressure loss coefficient overestimates the losses compared with the entropy loss coefficient.

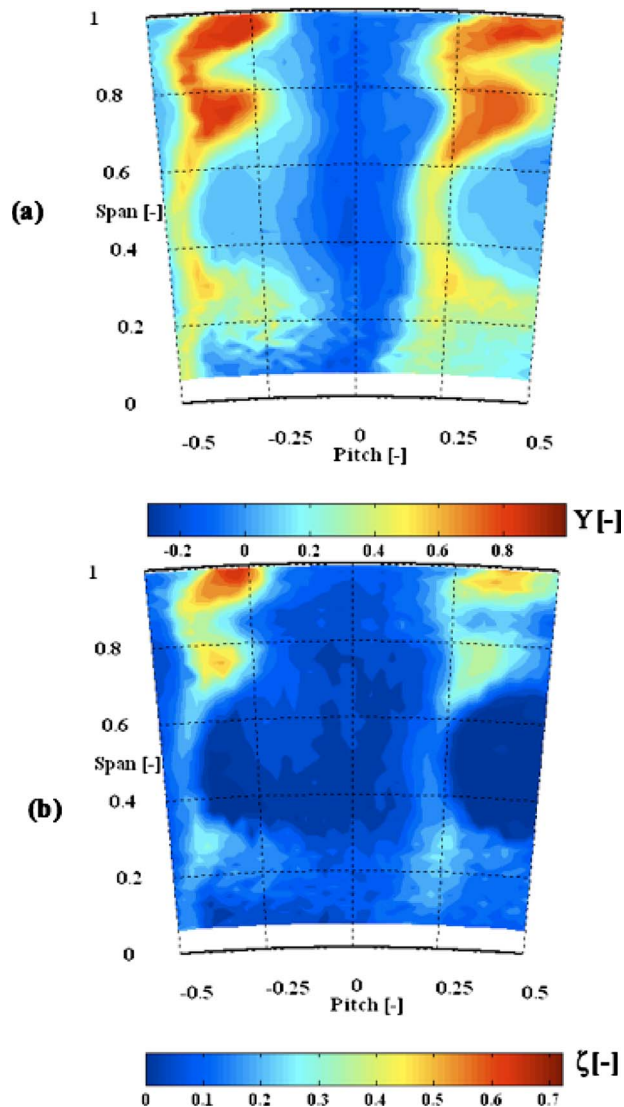


Fig. 6 Time-resolved stagnation (a) pressure loss coefficient and (b) entropy loss coefficient distribution at rotor exit

There is a tendency for the passage vortex and wake to separate and to migrate toward the suction side of the rotor blade, as described by the schematic model of Kerrebrock and Mikolajczak [21], and to increase in turbulence levels in the stator wake. In Fig. 7, it can be seen that the first stator passage vortex and wake have different relative velocities and thus different normal veloc-

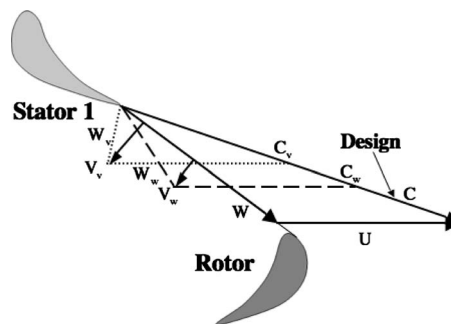


Fig. 7 Velocity triangles at stator exit for passage vortex and wake based on the kinematic model of Kerrebrock and Mikolajczak [21]

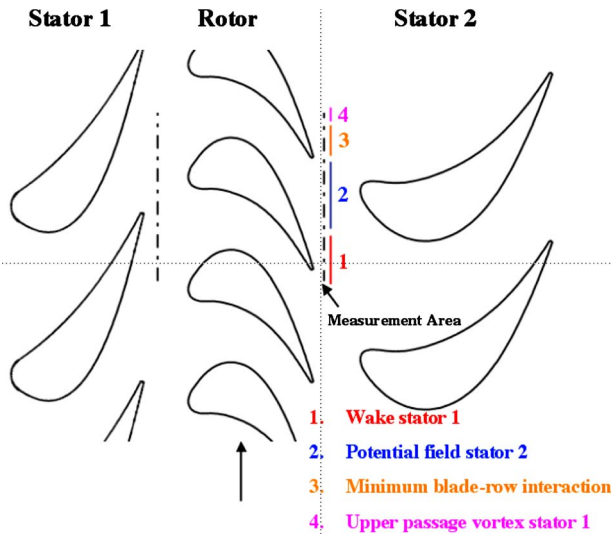


Fig. 8 Measurement plane at rotor exit. Numerals identify regions dominated by different types of unsteady blade row interaction.

ity components with respect to the suction side of the downstream rotor. Due to the different velocity deficits, the wake and passage vortices of the first stator appear at different times and positions at the rotor exit plane. This differential migration of the passage vortex and wake has an effect on the unsteady changes in both the secondary flow generation and the modulation of entropy creation.

Thus, in Fig. 8 the interaction regions that are dominated by the first stator wake and the first stator passage vortex are shown as regions 1 and 4, respectively. The region that is dominated by the potential field of the second stator is denoted as region 2; this interaction is strong due to the small gap, 30% of axial chord, between the blade rows. Lastly, region 3 denotes the region that has the minimum blade row interactions.

The radially averaged profiles that quantify the identification of the four interaction regions shown in Fig. 8 are presented in Figs. 9–11. The dominant potential field interaction that is centered on the midpitch results in the highest relative total pressure and relative total temperature, as seen in Fig. 9. The wake and passage vortex of the first stator can be identified from the plateaus in the relative total pressure; these plateaus are centered on the pitch

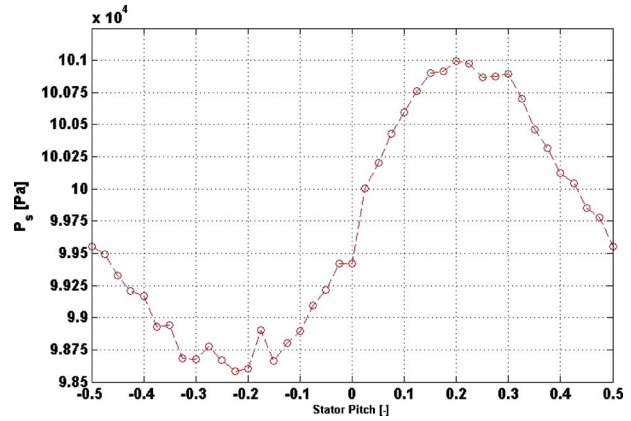


Fig. 10 Measured radially averaged static pressure at rotor exit

ranges of -0.35 to -0.2 and 0.4 – 0.5 , respectively. The signatures of these two features are not so pronounced in the relative total pressure profile. The radially averaged static pressure profile is shown in Fig. 10. This profile shows that relative to the mean static pressure at the rotor exit, the stator 1 wake is directed toward the suction side of the stator 2 blade.

The rms total pressure and the entropy function profiles are shown in Fig. 11. Porreca et al. [22] showed that the rms total pressure is a reliable measure of the turbulence intensity. Figure 11 shows that the stator 1 wake, pitch -0.35 to -0.2 , has the highest turbulence intensities and is also the lossiest region. The stator 1 passage vortex, pitch 0.4 – 0.5 , also has elevated levels of turbulence intensities but is not as lossy as the stator 1 wake.

The time-resolved flow field downstream of the rotor is presented in terms of the rms total pressure and the entropy function in Fig. 12. Three different instants of the rotor blade passing period, $t/T=0.0, 0.25$, and 0.5 , show the variation in the inter-blade-row interactions that affect the rotor secondary flow features and entropy creation. In each plot, the position of the second stator leading edge (SSLE) is shown as the vertical dotted line at mid-pitch, and its suction and pressure surfaces are to the left and right, respectively, of the midpitch.

At time $t/T=0$, the rotor passage vortices and tip leakage vortex are immediately ahead of the second stator leading edge; at this moment, the rotor secondary flow shows a minimum rms total

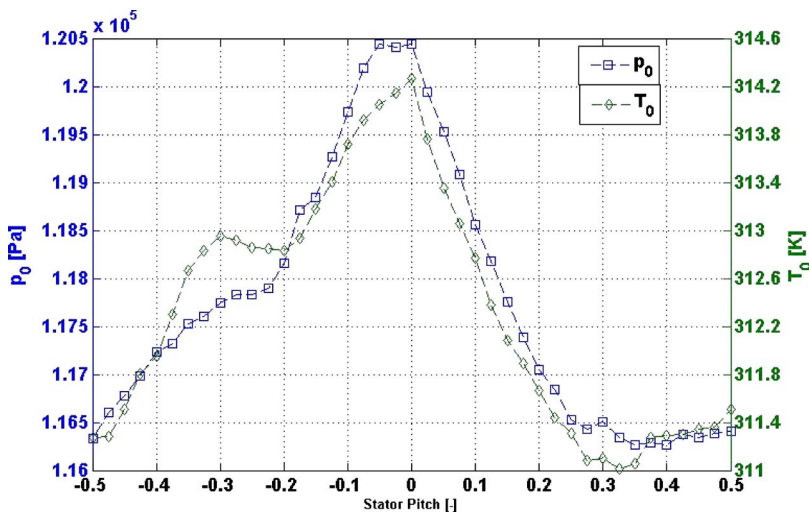


Fig. 9 Measured radially averaged relative total pressure and total temperature at rotor exit

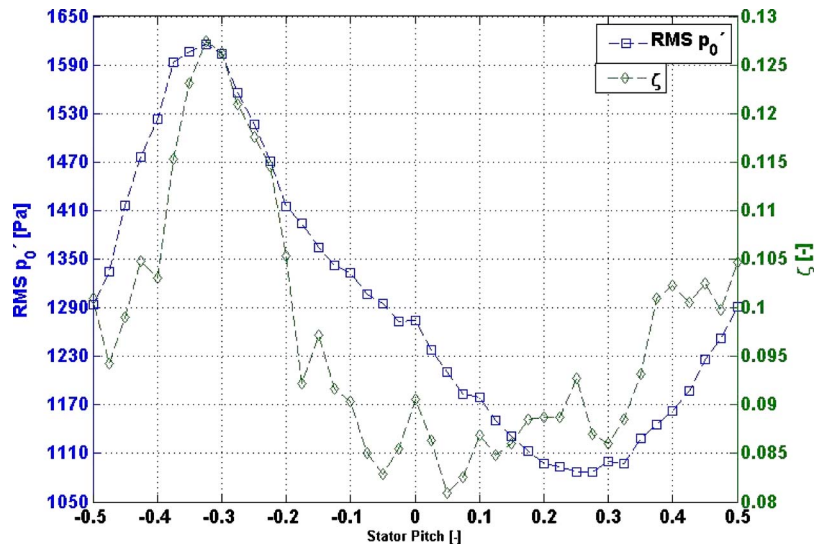


Fig. 11 Measured radially averaged rms of absolute total pressure and entropy function at rotor exit

pressure. The first stator wake is further from the second stator leading edge within the region that is bounded by the thick dotted perimeter line. It can be seen that the turbulence intensity and entropy generation in the first stator wake are less than those in the rotor secondary flow since the first stator wake has mixed out.

At time $t/T=0.25$, the turbulence intensity and entropy generation in the rotor secondary flow field are greater than those in the previous time period since it is now out of the potential field interaction zone. Within the square shown as a thick dotted line is a region of elevated turbulence intensity and entropy generation. Over a period, this feature appears periodically within this square area and then tends, first, to move toward the pressure surface of the second stator and then merges with the rotor upper passage vortex. It is suggested that this feature is associated with the first stator upper passage vortex. The incoming rotor secondary flow that is on the suction side of the second stator leading edge has an increase in entropy generation, especially pronounced in the tip region. This increase in entropy generation is a consequence of the strong interaction between the first stator wake and the rotor secondary flow.

At a later time, $t/T=0.50$, when the rotor upper passage vortex and first stator upper passage vortex have merged together, there is an increased level of turbulence intensity and entropy generation within the rotor upper passage vortex. The rotor tip leakage vortex is unaffected by the appearance of the first stator upper passage vortex. The incoming rotor secondary flow, pitch= -0.25 , is influenced by the leading edge of the second stator; thus, the vortices and wake are more closed spaced together.

It is evident from Fig. 12 that different secondary flow features at the rotor exit undergo modulations in the entropy generation. In order to describe this time variation in detail, four radial heights of 26%, 50%, 75%, and 90% spans are considered. At these heights, the behavior of the flow field is dominated by the rotor hub passage vortex (at 26% span), the rotor and first stator wakes (50% span), the rotor upper passage vortex (75% span), and the rotor tip gap vortex (95% span). At each height, a circumferential cut is considered, and the time variations of the turbulence intensity and entropy function are examined in Figs. 13–16. The time variations of the turbulence intensity and entropy function at 95% span are shown in Fig. 13. In these and all other space-time plots, the vertical dotted white line shows the circumferential position of the SSLE, and the diagonal white line shows the trajectory of the rotor trailing edge (RTE). The stator pitch range of -0.5 to -0.1 , within which the first stator wake periodically appears, is shown

as FSWS. The rotor tip leakage vortex is identified as the inclined region of the elevated turbulence intensity and entropy generation. The turbulence intensity and entropy generation are maximum at a stator pitch of -0.32 , which has previously been identified at the time mean position of the first stator wake. As the tip leakage vortex passes the second stator leading edge, it is first decelerated and then accelerated, while it expands circumferentially. This deceleration/acceleration results in a redistribution of the entropy generation around the second stator leading edge.

The time variation of entropy generation in the rotor upper passage vortex is examined in Fig. 14. Similar to the tip leakage vortex, the upper passage vortex has its maximum and minimum entropy generation during the interaction with the first stator wake and around the second stator leading edge, respectively. Furthermore, when the first stator upper passage vortex (FSPV) merges with the rotor passage vortex, the turbulence intensity decreases and the entropy generation increases.

In Fig. 15, the time variations of the turbulence intensity and entropy generation associated with the first stator wake are examined. The first stator wake can be seen in the region between two passing rotor blade wakes. In this region, the levels of turbulence intensity and entropy generation in the first stator wake are elevated but do not reach as high as the levels the rotor blade wakes subsequently reach due to heat transfer and mixing with the surrounding freestream. It is also interesting to note that as the first stator wake interacts with the rotor blade wakes, it largely moves toward the suction side of the rotor, and only a small portion remains adjacent to the pressure side. Hodson and Dawes [4] and Walreavens and Gallus [6] previously reported this behavior. A second interesting feature to observe is the marked increase in the entropy generation, which is also accompanied by an increase in the turbulence intensity, in the vicinity of midpitch. These increases are associated with the strong potential field interaction exerted by the second stator leading edge on the wake.

The time variations of the turbulence intensity and entropy function at 26% span that are associated with the rotor hub passage vortex are examined in Fig. 16. It should be noted that in the present configuration, air is injected from the hub rim seal between the first stator and the rotor stages to simulate purge flow. This injected flow enters over a pitch range of -0.4 to 0.05 , and its influence extends up to 35% span; thus, the turbulence intensities are increased over this pitch range, as seen in Fig. 16.

At the rotor exit (Fig. 8), four interaction zones that are based on the radially averaged pitchwise profiles have been identified.

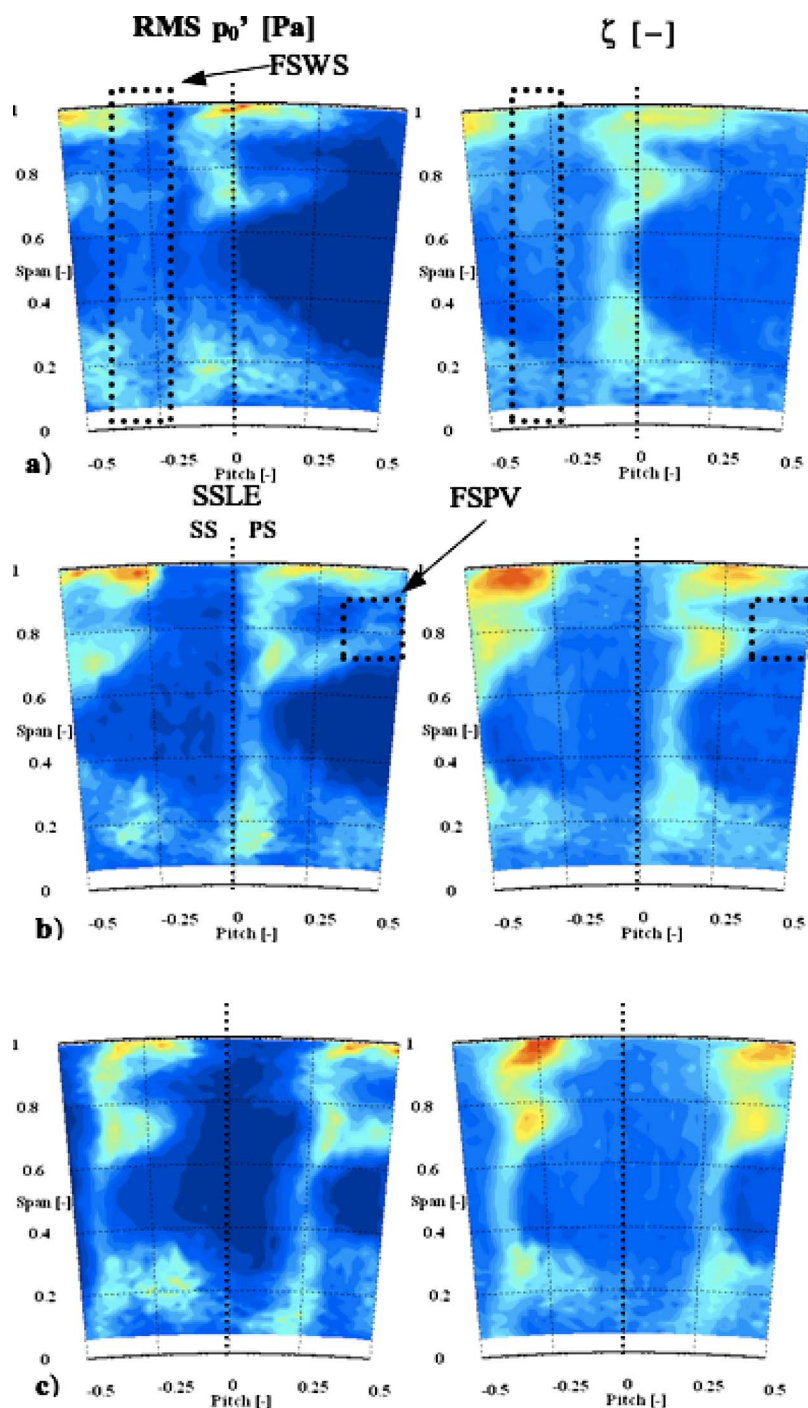


Fig. 12 rms total pressure (left column) and entropy loss coefficient (right column) distribution behind the rotor at three instants of the rotor blade passing period: (a) $t/T=0.00$, (b) $t/T=0.25$, and (c) $t/T=0.50$

The time-resolved entropy generation in each of the zones is next examined from the spanwise profiles at -0.32 , 0.0 , 0.30 , and 0.5 pitch (Fig. 17). The plots are viewed in the downstream direction, and each plot covers three rotor passages. It is evident that the rotor tip leakage vortex and the passage vortices have the largest modulations in entropy generation. The entropy generation is maximum when these vortices interact with the first stator wake (Fig. 17(a)) and is minimum when the vortices are immediately in front of the second stator leading edge (Fig. 17(b)). The rotor

wake and hub passage vortex have smaller modulations of entropy generation, although we note again that the hub passage vortex is modified by simulated purge flow.

For comparison, the time-resolved spanwise profiles of relative stagnation pressure loss coefficient are plotted in Fig. 18. The stagnation pressure loss coefficient captures the modulation of the loss in the rotor secondary flow field. However, the stagnation pressure loss coefficient is underestimated between the rotor secondary flows at both -0.32 and midpitch. At -0.32 pitch, the

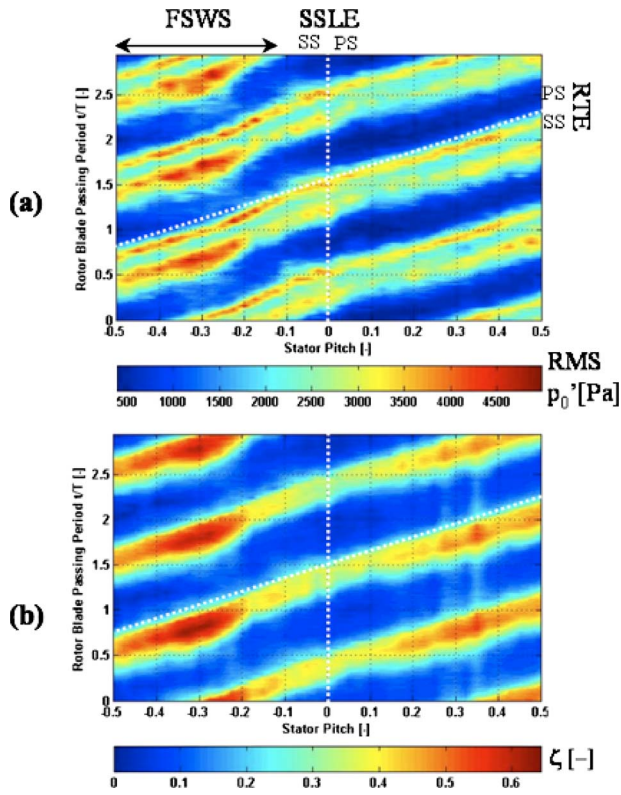


Fig. 13 Circumferential distribution of (a) rms total pressure and (b) entropy function versus time at rotor exit for 95% span

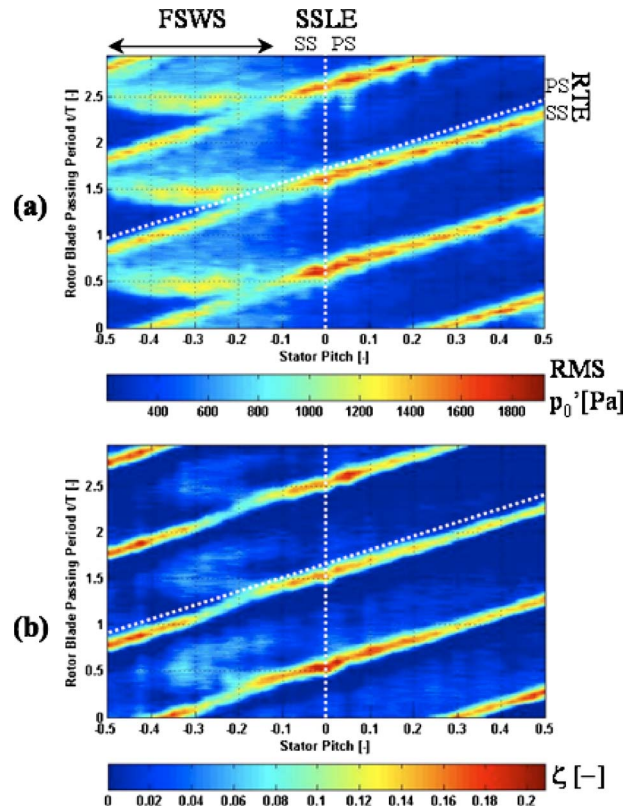


Fig. 15 Circumferential distribution of (a) rms total pressure and (b) entropy function versus time at rotor exit for 50% span

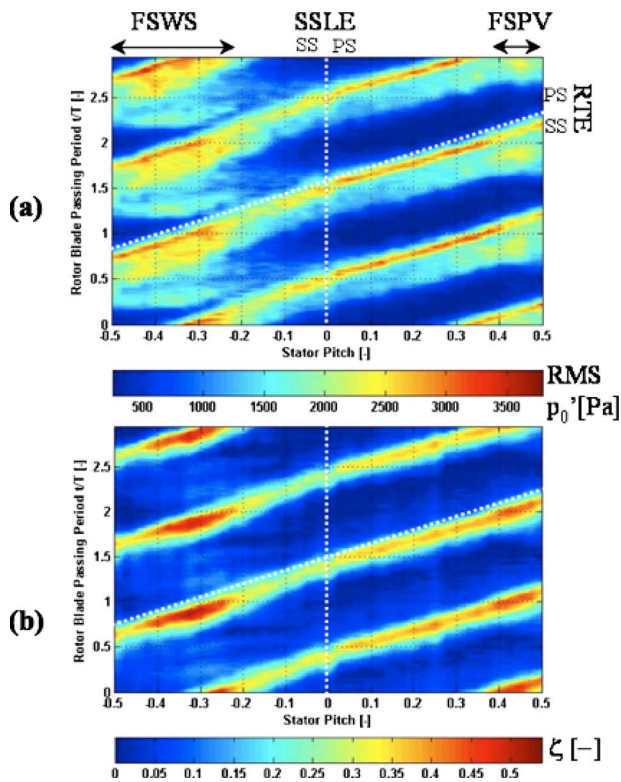


Fig. 14 Circumferential distribution of (a) rms total pressure and (b) entropy function versus time at rotor exit for 75% span

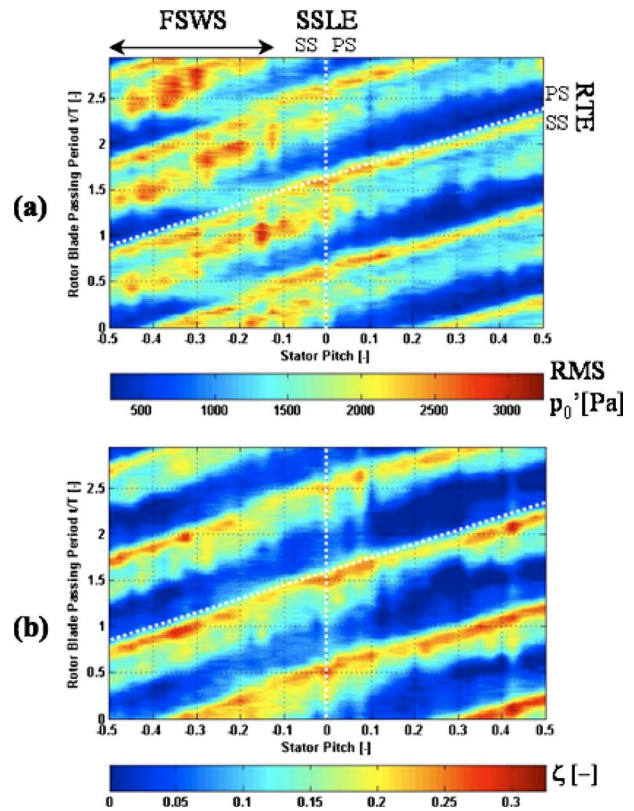


Fig. 16 Circumferential distribution of (a) rms total pressure and (b) entropy function versus time at rotor exit for 26% span

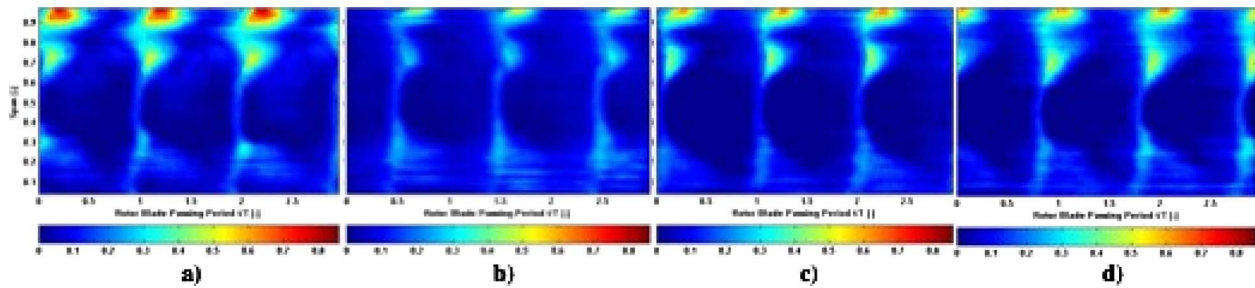


Fig. 17 Time-resolved, spanwise profiles of entropy loss coefficient at (a) -0.32 pitch, (b) 0 pitch, (c) 0.3 pitch, and (d) 0.45 pitch. Pitchwise locations correspond to interaction zones identified in Fig. 8.

high relative total pressure occurs due to the presence of the first stator wake, which has done less work than the freestream through the rotor. At midpitch, the high relative total pressure in the freestream is the result of the potential field of the second stator. Thus, in the freestream, the losses are underestimated at -0.32 pitch and midpitch and are overestimated at 0.3 and 0.45 pitch.

Figure 19 presents the time-averaged profiles of the entropy loss coefficient at each of the interaction zones. The results show that in each interaction zone, the rotor tip vortex, 0.9 – 1.0 span, has the largest entropy generation, whereas the rotor wake region, 0.35 – 0.6 span, has the lowest entropy generation. In the interaction zone that is dominated by the first stator wake and passage vortex, the rotor upper passage vortex, 0.7 – 0.8 span, is more lossy than the rotor lower passage vortex (0.3 – 0.1 span), whereas at midpitch where the interaction with the second stator potential field and the injected air from the hub rim seal are strong, the reverse is true.

It is useful now to conclude with the loss generation audits in each interaction zone. The loss generation audits are shown in Fig. 20 and are based on the spanwise regions that are summarized in Table 3. The loss generation audit is determined as the difference between the entropy loss in the interaction zone and the pitchwise-averaged value; the pitchwise-averaged values shown in Fig. 4 are used for normalization. It can be seen that in the TLV region the largest fluctuation (71%) relative to the pitchwise-averaged loss occurs. The losses are increased by more than 47% when there is an interaction that is dominated by the first stator wake and then reduced by 23% in the presence of the second stator's potential field. The modulations associated with the UPV region vary similarly to the TLV, but with smaller amplitudes. The losses in the upper passage vortex region increase by 39% when interacting with the first stator wake and by 14% when there is an interaction with the second stator tip vortex. In the presence of the potential field of the second stator, the losses decrease by 19% . The wake region has a largest modulation in entropy generation of 25.8% at the midpitch. On the other hand, the minimum modulation of -37.7% occurs when the blade row interaction is minimum. The

least sensitivity to the inter-blade-row interactions is observed in the LPV region. The modulation in loss generation is 32% , with an increase of 18% measured at midpitch.

5 Concluding Remarks

The measurements of the unsteady entropy field at the rotor exit of a one-and-one-half-stage turbine model, which is representative of a highly loaded, high-pressure stage of an aero-engine, have been presented. The measurements are made with a novel miniature fast-response entropy probe that has been developed at ETH Zurich. The probe integrates a fast-response aerodynamic probe and a pair of thin-film gauges from which the time-resolved entropy can be determined.

The measurements of the unsteady entropy field that is associated with the inter-blade-row interactions are described in detail. These measurements indicate that there are pitchwise and spanwise variations in the total pressure and total temperature. As result of these variations, there is a significant modulation of the unsteady loss at the rotor exit flow field. The different contributions to this modulation from the stator wake interaction, the secondary flow interaction, and the potential field interaction are described. This improved understanding can assist a designer in modifying features of the flow that are most responsible for the unsteady loss generation.

The quantifications of the blade losses in terms of an entropy loss coefficient and a stagnation pressure loss coefficient are compared. For the present turbine model configuration, the overall losses and distribution of losses are misrepresented by the stagnation pressure loss coefficient. The overall losses are overestimated by more than 69% using the stagnation pressure loss coefficient. Furthermore, the entropy loss coefficient identifies the tip leakage vortex as the most lossy region, followed by the lower passage vortex, and then the upper passage vortex. On the other hand, in terms of the stagnation pressure loss coefficient, the order of decreasing loss generation is as follows: lower passage vortex, upper passage vortex, and tip leakage vortex.

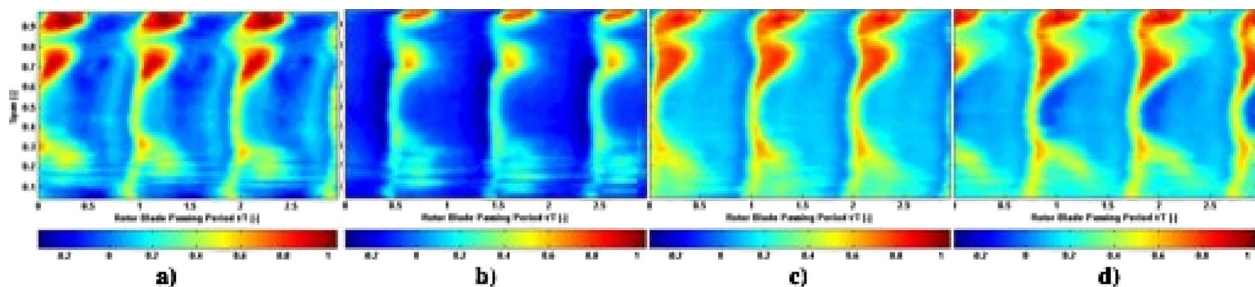


Fig. 18 Time-resolved, spanwise profiles of stagnation pressure loss coefficient at (a) -0.32 pitch, (b) 0 pitch, (c) 0.3 pitch, and (d) 0.5 pitch. Pitchwise locations correspond to interaction zones identified in Fig. 8.

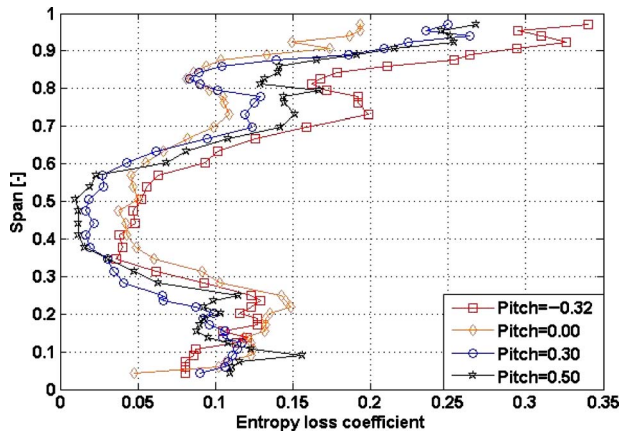


Fig. 19 Time-averaged spanwise profiles of entropy loss coefficient for traverses at the four interaction zones shown in Fig. 8

Based on the entropy loss coefficient, the interaction of the rotor tip leakage and upper passage vortices with the upstream stator wake structure is responsible for an increased loss of +48% and +39% above the pitchwise-averaged loss, whereas the rotor lower passage vortex is rather insensitive to the stator wake. On the other hand, the potential field of the downstream stator tends to reduce the losses in the rotor tip leakage and upper passage vortex, -23% and -19%, respectively, but increases the losses of the wake (+35%). As the rotor tip leakage and upper passage vortices are overall the lossiest regions, the modulations of their absolute losses are the most significant with regard to the time-varying behavior of this turbine.

The significance of these differences is that from the perspective of a designer, the entropy loss coefficient provides a more reliable measure of loss than the stagnation pressure loss coefficient. These differences are found in the present axial research turbine, which is a relatively low temperature turbine. Even so, in this facility, the effects of heat transfer and unsteady work are measurable and non-negligible. We anticipate that these effects will be much more pronounced in higher temperature facilities, including full-scale gas turbine engines.

Acknowledgment

The authors acknowledge the support of Peter Schüpbach in helping to conduct the measurements in LISA. The authors also

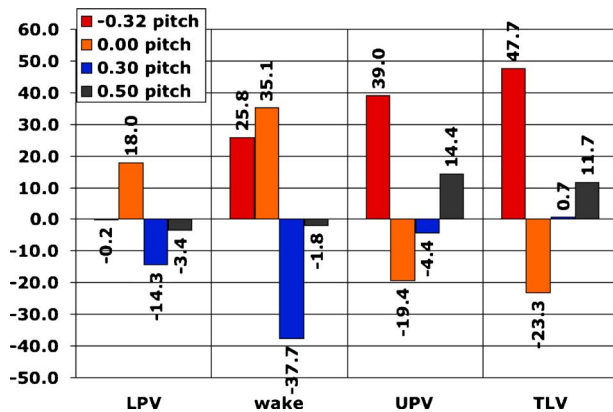


Fig. 20 Modulation in entropy generation rate at different pitch positions at the rotor exit measurement plane as a percentage of the pitchwise-averaged entropy loss coefficient

thank Cornel Reshef for his work in developing the electronic instrumentation and data acquisition system for the fast-response entropy probe.

Nomenclature

- c_p = specific heat
- c = absolute velocity
- Δp_o = total pressure difference, $p_{01} - p_{02}$
- ΔT_o = total temperature difference, $T_{01} - T_{02}$
- Nu = Nusselt number
- p = pressure
- p'_o = rms total pressure, $p(t) - \bar{p} - \tilde{p}(t)$
- R = gas constant, resistance
- Δs = relative entropy
- t = time
- T = temperature
- t/T = blade passing period
- T_2 = static temperature at the rotor exit
- u = rotational speed
- v = normal component of velocity
- w = relative velocity
- $w_{2,max}$ = maximum relative velocity at rotor exit

Greek

- Y = stagnation pressure loss coefficient, $(p_{01} - p_{02}) / (0.5 \rho w_{2,max}^2)$
- ϕ = flow coefficient, c_x / u
- ψ = loading coefficient, $\Delta h / u^2$
- ζ = entropy loss coefficient, $T_2 \Delta s / (0.5 w_{2,max}^2)$

Superscripts

- ' = random part
- = average
- ~ = periodic

Subscripts

- 1 = rotor inlet
- 2 = rotor outlet
- f = freestream
- max = maximum
- o = total
- ref = reference condition
- s = static
- v = passage vortex
- w = relative
- w = wake
- x = axial direction

Abbreviations

- FENT = fast-response entropy probe
- FSPV = first stator passage vortex
- FSWS = first stator wake structure
- LPV = lower passage vortex
- MP = measurement plane
- PS = pressure side
- rms = root mean square
- RTE = rotor trailing edge
- SS = suction side
- SSLE = second stator leading edge
- TLV = tip leakage vortex
- UPV = upper passage vortex

References

- [1] Wisler, D. C., 1998, "The Technical and Economic Relevance of Understanding Blade Row Interaction Effects in Turbomachinery," *Blade Row Interaction Effects in Axial Turbomachinery Stages* (VKI LS 1998-02), von Karman Institute for Fluid Dynamics, Rhode-St. Genèse, Belgium.
- [2] Sharma, O. P., Pickett, G. F., and Ni, R. H., 1992, "Assessment of Unsteady Flows in Turbines," *ASME J. Turbomach.*, **114**, pp. 79-90.
- [3] Binder, A., Forster, W., Mach, K., and Rogge, H., 1986, "Unsteady Flow

- Interaction Caused by Stator Secondary Vortices in a Turbine Rotor,” ASME Paper No. 86-GT-302.
- [4] Hodson, H. P., and Dawes, W. N., 1998, “On the Interpretation of Measured Profile Losses in Unsteady-Turbine Blade Interaction Studies,” *ASME J. Turbomach.*, **120**, pp. 276–284.
- [5] Miller, R. J., Moss, R. W., Ainsworth, R. W., and Horwood, C. K., 2003, “Time-Resolved Vane-Rotor Interaction in a High-Pressure Turbine Stage,” *ASME J. Turbomach.*, **125**, pp. 1–13.
- [6] Walreavens, R. E., and Gallus, H. E., 1995, “Stator–Rotor–Stator Interaction in an Axial Flow Turbine and Its Influence on Loss Mechanisms,” AGARD-CP-571, 85th Meeting on Loss Mechanisms and Unsteady Flows in Turbomachinery, Paper No. 39.
- [7] Greitzer, E. M., Tan, C. S., and Graf, M. B., 2004, *Internal Flow: Concepts and Applications*, Cambridge University Press, Cambridge, UK.
- [8] Denton, J. D., 1993, “Loss Mechanisms in Turbomachines,” *ASME J. Turbomach.*, **115**, pp. 621–652.
- [9] Ng, W. F., and Epstein, A. H., 1984, “Unsteady Losses in Transonic Compressors,” ASME Paper No. 84-GT-183.
- [10] Payne, S. J., Ainsworth, R. W., Miller, R. J., Moss, R. W., and Harvey, N. W., 2003, “Unsteady Loss in a High Pressure Turbine Stage,” *Int. J. Heat Fluid Flow*, **24**, pp. 698–708.
- [11] Brouckart, J. F., 1998, “Experience With a Double-Hot-Wire Aspirating Probe in a Transonic Turbine Stage,” *Proceedings of the 14th Symposium on Measuring Technique for Transonic and Supersonic Flows Cascades in Turbomachines*, Limerick.
- [12] Buttsworth, D. R., Jones, T. V., and Chana, K. S., 1998, “Unsteady Total Temperature Measurements Downstream of a High-Pressure Turbine,” *ASME J. Turbomach.*, **120**, pp. 760–766.
- [13] Buttsworth, D. R., and Jones, T. V., 1998, “A Fast-Response High Spatial Resolution Total Temperature Probe Using a Pulsed Heating Technique,” *ASME J. Turbomach.*, **120**, pp. 601–607.
- [14] Passaro, A., LaGraff, J. E., Oldfield, M. L. G., Biagioni, L., Moss, R. W., and Battelle, R. J., 2003, “Measurements of Turbulent Pressure and Temperature Fluctuation in Gas Turbine Combustor,” NASA, Report No. NASA-CR-2003-212540.
- [15] Chana, K. S., 2004, “Requirements for Instrumentation Technology for Gas Turbine Propulsion Systems—Gas Total Surface Temperature Measurements for Harsh Environments,” *Advanced Measurement Techniques for Aeroengines and Stationary Gas Turbines* (VKI LS 2004–04), von Karman Institute for Fluid Dynamics, Rhode-St. Genèse, Belgium.
- [16] Mansour, M., Chokani, N., Kalfas, A. I., and Abhari, R. S., 2008, “Unsteady Entropy Measurements in a High-Speed Radial Compressor,” *ASME J. Eng. Gas Turbines Power*, **130**, p. 021603.
- [17] Behr, T., Kalfas, A. I., and Abhari, R. S., 2007, “Unsteady Flow Physics and Performance of a One-and-1/2-Stage Unshrouded High Work Turbine,” *ASME J. Turbomach.*, **129**, pp. 348–359.
- [18] Schuepbach, P., Abhari, R. S., Rose, M. G., Germain, T., Raab, I., and Gier, J., 2008, “Performance Sensitivity of a High Work Turbine to Purge Flow and Endwall Profiling,” ASME Paper No. 2008-GT-50471.
- [19] Chaluvadi, V. S. P., Kalfas, A. I., Hodson, H. P., Ohyama, H., and Watanabe, E., 2003, “Blade Row Interaction in a High-Pressure Steam Turbine,” *ASME J. Turbomach.*, **125**, pp. 14–24.
- [20] Schuepbach, P., Abhari, R. S., Rose, M. G., Germain, T., Raab, I., and Gier, J., 2008, “Improving Efficiency of a High Work Turbine Using Non-Axisymmetric Endwalls. Part II: Time-Resolved Flow Physics,” ASME Paper No. 2008-GT-50470.
- [21] Kerrebrock, J. L., and Mikolajczak, A. A., 1970, “Intra Stator Transport of Rotor Wakes and Its Effect on Compressor Performance,” *ASME J. Eng. Power*, **92**, pp. 359–370.
- [22] Porreca, L., Hollenstein, M., Kalfas, A., and Abhari, R., 2007, “Turbulence Measurements and Analysis in a Multistage Axial Turbine,” *J. Propul. Power*, **23**, pp. 227–234.